This item is the archived peer-reviewed author-version of:

Into a rapid polymer characterization employing optical measurement systems and high-power ultrasonic excitation

Into a rapid polymer characterization employing optical measurement systems and high-power ultrasonic excitation.

Navid Hasheminejad [a,*], Steve Vanlanduit [b], Taher Ghalandari [a], Fabrice Pierron [c,d], Cedric Vuye [a]

[a] *University of Antwerp, SuPAR Research Group, Faculty of Applied Engineering, Groenenborgerlaan 171, Antwerp 2020, Belgium*

[b] *University of Antwerp, InViLab Research Group, Faculty of Applied Engineering, Groenenborgerlaan 171, Antwerp 2020, Belgium*

[c] *MatchID NV, Leiekaai 25A, Gent 9000, Belgium*

[d] *University of Southampton, Faculty of Engineering and Physical Sciences, Southampton, UK*

Abstract

This study presents a novel methodology for estimating the master curve of the complex modulus of viscoelastic materials using a combination of optical measurement systems and ultrasonic excitation. Traditional techniques for characterizing properties of viscoelastic materials are often time-consuming and encounter limitations that hinder their accuracy at high strain rates. To address this, a method was proposed that leverages two optical measurement systems to quickly assess material properties at multiple points on a sample. A high-power ultrasonic transducer was employed to excite the material at its first longitudinal natural frequency, creating non-uniform temperature variations and strain rates. A scanning laser Doppler vibrometer measured vibrations across the material, enabling computation of the complex modulus magnitude under varying conditions. These results were correlated with temperature readings obtained from an infrared camera. The constructed master curve using the proposed methodology closely resembled those established through quasi-static and dynamic uniaxial compression tests in the literature. Additionally, this method revealed a more substantial increase in complex modulus at high strain rates compared to traditional experiments, where this characteristic is less pronounced.

Keywords: ultrasonic excitation - complex modulus - polymethyl methacrylate (PMMA) - continuous scan laser Doppler vibrometry (CSLDV) - Infrared thermography

1. Introduction

Characterizing the mechanical properties of viscoelastic materials such as polymers is important in various industries and applications. Over time, several experimental techniques have been proposed to characterize the mechanical behavior of polymers as a function of temperature and strain rate [1,2]. Depending on the methodology, excitation and measurement system used, these experiments often focus on specific temperature and strain rate ranges. These techniques often rely on conventional sensors such as stain gauges or point velocity measurements, which limits the available data and testing capabilities. A detailed overview of these established techniques and their corresponding strain rate ranges is presented in a comprehensive review article by Siviour *et al.* [3].

However, with the rapid advancements in computer technology and optical measurement systems over the last few decades, innovative methods have emerged that use full-field measurements to characterize the mechanical properties of the materials. These tests rely on more complex configurations with respect to the traditional methods and exploit the full-field data and inverse identification to find the properties of the materials [4]. Such tests are named "Material testing 2.0" by some researchers, signifying a comprehensive transformation of traditional mechanical testing practices. This evolution is anticipated to eventually lead to the establishment of new standards as optical measurement systems progressively replace strain gauges and extensometers in testing laboratories [5].

32   Among these novel techniques is the image-based ultrasonic shaking (IBUS) test which uses ultra-high-speed
33   imaging and infrared thermography to estimate the complex modulus master curve of materials. This method
34   focuses on tests performed with high strain rates and above room temperature [6]. In this approach, the full-field
35   accelerations are calculated and used as image-embedded load cells to find the stiffness of the material without
36   external measurement of the applied force [7]. In this test, vibration-induced heating [8] (self-heating or hysteretic
37   heating) is taken advantage of to heat the sample during the experiments and create a temperature variation along
38   the sample. In many materials, including polymeric materials, internal damping can induce significant self-heating
39   during dynamic deformations, especially at high frequencies [9,10].

40   Another optical measurement system that has been used in the literature to characterize the mechanical
41   properties of viscoelastic materials is the Scanning Laser Doppler Vibrometer (SLDV) [11,12]. In these works,
42   SLDVs are typically employed to conduct out-of-plane vibration measurements and determine material properties
43   through modal analysis. This means that similar to traditional techniques, these experiments have to be conducted
44   at multiple temperatures to construct a comprehensive master curve of complex modulus, which makes these tests
45   extremely time-consuming [12]. Consequently, there exists a gap in the literature concerning the application of an
46   SLDV in combination with a high-power ultrasonic transducer to estimate the full master curve of the material with
47   a quick experiment. The SLDV's competitive sampling rate and precise resolution make it a compelling choice for
48   such measurements compared to a high-speed camera [13].

49   SLDVs offer two primary methods for conducting measurements on materials. The first involves creating a
50   predefined grid on the sample and scanning each point individually [14]. The second method entails continuous
51   scanning along a defined line [15,16]. The second approach, known as Continuous Scanning Laser Doppler
52   Vibrometry (CSLDV), combines the temporal oscillation and spatial distribution of the deflection into a single
53   output-modulated signal where the harmonic oscillation and spatial distribution across a swept area are defined by
54   a central harmonic and its sidebands [17]. The advantage of using this approach with respect to point-by-point
55   scans on a grid is an increased measurement resolution with a drastically decreased measurement time [13].

56   In this research, an innovative methodology was devised that utilizes ultrasonic excitation and integrates two
57   optical measurement techniques: infrared thermography and CSLDV. Furthermore, the necessary data processing
58   techniques for constructing the complex modulus master curve of a polymethyl methacrylate (PMMA) sample
59   based on these measurements were developed. The full-field acceleration was used to calculate the stress instead
60   of traditional load cells. The development of this novel technique leads to the construction of the complex modulus
61   master curve in a few minutes for a wide range of reduced frequencies. This paper primarily emphasizes on the
62   development of the experimental setup and data processing and the findings were compared with those reported in
63   the literature.

64   This paper is structured as follows. Section 2 details the experimental setup and data processing techniques for
65   analyzing the measurements. Section 3 presents the results of the proposed experiment and the comparison of the
66   estimated master curves with results from the literature. Finally, research conclusions and possibilities for future
67   work are provided in Section 4.

68

69   2. Materials and methods

70   2.1. Sample preparation

71   The material selected for this research was polymethyl methacrylate (PMMA, also known as cast acrylic). The
72   sample, measuring 4.1 mm in thickness, 11.8 mm in width, and 54.5 mm in length, was laser-cut from a plate
73   sourced from IMATEX N.V. (Belgium). This specific sample length A was chosen according to Eq. 1 to ensure
74   that its first longitudinal natural frequency closely aligns with the excitation frequency of the transducer used. The
75   excitation frequency of this transducer is near a particular frequency, as elaborated in Sections 2.2.1 and 2.4.
76

$$A = \frac{1}{2f}\sqrt{E/\rho} \tag{1}$$

with *f* the excitation frequency, *E* the modulus of elasticity of the material, and *ρ* the density of the material. The comprehensive properties of the PMMA used in this research, obtained from its datasheet, are summarized in Table 1.

Table 1: Properties of the PMMA sample

Density [g/cm^3]	1.19
Young's modulus – quasi-static (GPa)	3.3
Vicat softening temperature B50 [°C]	115

The PMMA used in this study was in its natural transparent state. Therefore, in order to prepare it for LDV measurements, the material's surface underwent a two-step painting process. Initially, a layer of matte black paint was applied, followed by an additional application of white spray paint (Ardrox® 9D1B aerosol). This guarantees a high level of reflection for the emitted laser onto the sample surface [18].

2.2. Experimental setup

The goal was to induce a range of strain rates and temperatures within the PMMA sample. This was achieved by utilizing a high-power ultrasound transducer to create a range of strain rates and temperatures necessary for constructing the master curve of the complex modulus. Simultaneously, surface vibration and temperature were monitored using an SLDV and a thermal camera (see Figure 1: Schematic representation of the proposed experimental setup). The following provides a detailed description of each equipment used in the setup.
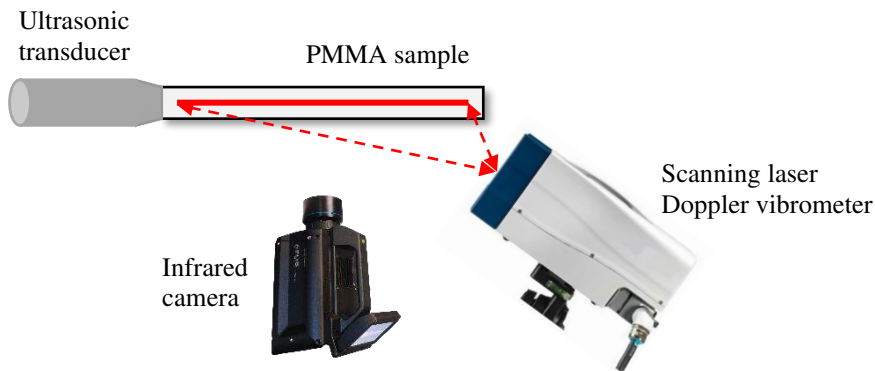

Figure 1: Schematic representation of the proposed experimental setup

2.2.1. High-power ultrasonic transducer
Following preliminary experiments using a modal shaker to excite the specimen, it was concluded that an excitation source with higher power is needed to achieve the required range of strain rate and induce temperature variations within the sample [19]. In line with this requirement, a high-power ultrasonic transducer was employed for this research. Specifically, the NexTgen Lab750 generator, coupled with the 40D13 axial probe from SynapTec (France), previously used by [6] was selected for this setup. This transducer is engineered to generate a harmonic signal with a frequency close to 20 kHz and a peak-to-peak displacement amplitude of 140 μm, as outlined in its

100   datasheets. Moreover, the surface of the output horn of the transducer has a diameter of 13 mm, a parameter which
101   sets the maximum width of the sample attached to the transducer.

2.2.2. Scanning laser Doppler vibrometer

103   To measure the vibration on the surface of the sample, a He-Ne PSV-400 SLDV from Polytec (Germany) was
104   employed. This device effectively measures the velocity on the surface of the material with a maximum sampling
105   rate of 204.8 kHz using its VD-03 decoder. This system operates with a class 2 laser at a 633 nm wavelength and
106   less than 1 mW power.
107   Typically, a single-head SLDV is employed for capturing out-of-plane vibrations in specimens. In our study,
108   however, the SLDV was positioned at a specific angle (30°) with respect to the specimen, allowing for measurement
109   and subsequent correction of in-plane vibrations based on this angle. This is only possible if the out-of-plane
110   vibration of the specimen is assumed to be negligible.
111   Traditionally, the SLDV conducts measurements across a predefined grid on the surface of the object. However,
112   as shown in Section 2.4, stress determination requires simultaneous acceleration measurements across the entire
113   surface. This poses challenges, especially considering temperature fluctuations during experimentation and the
114   impracticality of point-by-point measurements during loading. To address this, two techniques are considered.
115   The first technique involves conducting fast point-by-point scanning. However, the PSV-400 SLDV's software
116   necessitates a stabilization period following each laser movement, rendering rapid measurements unfeasible and
117   increasing the sampling time. The second technique, which was used in this research, employs CSLDV, a method
118   well-established for flat surfaces perpendicular to the laser beam [17]. Given the angle between the sample and
119   laser beam in the developed setup, an alternate approach has been adopted for data analysis of the CSLDV
120   measurements (see Section 2.4 for comprehensive details). To establish this method, the generator of the SLDV
121   was connected to the galvo scanner of the SLDV, and a sinusoidal signal with a 5 Hz frequency was introduced to
122   the vertical galvo scanner. If required, this galvo scanner can be excited to achieve frequencies of up to 100 Hz. To
123   synchronize the vibration measurements with laser positioning, a trigger was implemented on the input signal of
124   the galvo scanner to initiate measurements simultaneously.

2.2.3. High-Speed midwave IR camera

126   A FLIR X6540sc camera with a spectral range of 1.5 – 5.5 µm, coupled with a 25 mm – 22° x 17° lens, was
127   utilized for thermal imaging in this research. This camera provides 640 x 512 full-frame images at a high frame
128   rate of up to 355 Hz while maintaining a short integration time crucial for accurately capturing rapid processes.
129   User-defined subwindowing allows for even faster frame rates, up to 4500 Hz. During the experiments, a specific
130   configuration of a 600 x 60-pixel window and a frame rate of 50 Hz was selected, and the temperatures in between
131   were interpolated.
132   The FLIR X6540sc camera interfaces with the FLIR ResearchIR Max software provided for visualizing and
133   processing thermal data. The output was transferred to MATLAB and further analyzed using developed codes. This
134   camera has a noise equivalent differential temperature below 25 mK (20 mK typical), and its standard temperature
135   range extends from 5°C to 300°C, facilitating measurements across a broad thermal spectrum. Throughout the
136   various test stages, distinct integration times were employed to cover specific temperature ranges: 626 µs for the
137   range of 5 - 93°C, 478 µs for the range of 20 - 115°C, and 359 µs for the range of 40 - 130°C. This tailored approach
138   to integration times ensured accurate thermal measurements across diverse temperature scenarios.
139   To synchronize the camera with the SLDV, a trigger was configured using the output of the generator signal
140   used to control the galvo scanner. Further processing of the acquired images is discussed in detail in section 2.4.

2.2.4. Cold air chiller device

142   In order to broaden the range of the available data to encompass temperatures below room temperature, the
143   experimental setup included a Cryo 6 cold air chiller manufactured by Zimmer MedizinSysteme (Germany). This
144   device is designed to deliver cold air with the capability to reach as low as -30°C, precisely targeted at the

145 designated area through a connected hose. The application of the Cryo 6 cold air chiller was limited to only a
146 specific phase of the experiments (Step 6, refer to Table 2). During this phase, the device effectively reduced the
147 sample's temperature from 23°C to between 6 and 10°C within a span of around 3 minutes. The addition of this
148 phase allowed for the formation of the master curve in a wider temperature range.

149 *2.3. Experimental procedure*

150 Once the sample was prepared, it was glued to the horn of the ultrasonic transducer using a Bison superglue in
151 gel form. The transducer was then mounted on a dedicated stand. For vibration measurements, the SLDV was
152 positioned at a precise 30° angle relative to the surface of the sample and a distance of 1.12 m from the center of
153 the sample. This angle selection ensured in-plane vibration measurements while the distance adhered to the optimal
154 stand-off distance formula as prescribed by the hardware manual of the device. The overview of the experimental
155 setup is depicted in Figure 2. During the measurement process, the galvo scanner of the SLDV was stimulated by
156 a sinusoidal signal with a frequency of 5 Hz. The amplitude of this signal was adjusted to generate a scanning line
157 of 5 cm along the middle of the sample in horizontal direction. Considering the frequency of the galvo scanner
158 (5 Hz) and the sampling rate of the SLDV (204.8 kHz), a total of 20480 data points were recorded along the
159 scanning line during each pass of the laser. Lastly, the IR camera was positioned in front of the sample.
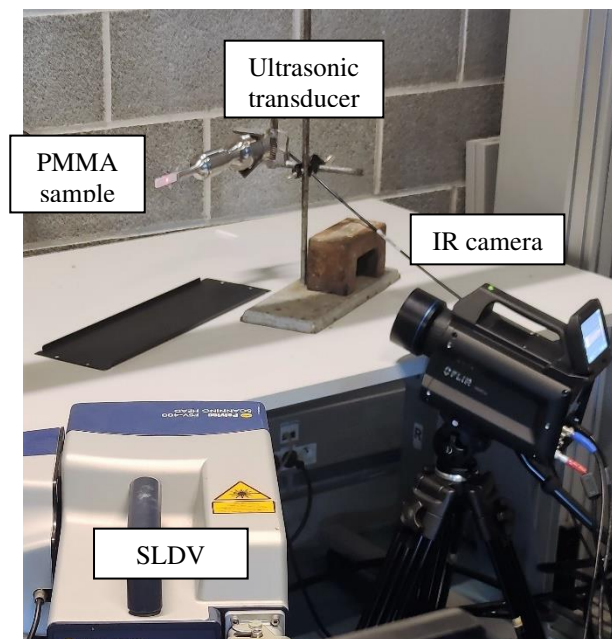160

Figure 2: Overview of the experimental setup

161
162 The experiments were performed in a sequence of steps. In each step, the ultrasonic transducer applied a
163 15-second excitation at 15% power, followed by a designated resting interval. A comprehensive breakdown of each
164 step of the experiment is presented in Table 2. As evident, the final step involved a 3-minute cooling period
165 beforehand.
166

167 Table 2: Experimental procedure and the temperature on the surface at each step of the test

	Surface temperature range in °C		Waiting time after
	Before excitation	After excitation	
Step 1	23	23-52	3 min
Step 2	23-31	24-67	3 min
Step 3	23-40	24-86	2 min
Step 4	23-46	24-100	1 min
Step 5	24-68	24-117	1 hour + 3 min cooling
Step 6	6-10	9-25	-

* Each step includes a 15-second excitation at 15% power

168

169 *2.4. Data processing*

170   The measured velocity along the laser beam was adjusted based on the angle between the laser beam and the
171 surface of the sample. A uniform correction angle of 30° was applied across the entire scanning line since the
172 distance of the SLDV from the sample is much larger than the length of the sample.
173   Additionally, the positional coordinates of the laser spot on the sample can be determined at any given moment
174 using the mirror's angle (α), as outlined in Equation 2:

$$loc = \frac{d \sin(\alpha)}{\sin(ang - \alpha)} \tag{2}$$

175 with d representing the distance between the SLDV mirror and the center of the sample, equal to 1.12 m in this
176 case, and ang denoting the angle between the laser beam and the sample's midpoint, which was 30° for this
177 experiment.
178   Figure 3 demonstrates an exemplary measured velocity signal, along with the position of the laser spot on a line
179 along the sample. It is important to note that due to the time delay between the mirror position and its input drive
180 signal in practice [20], manual adjustment of the trigger point had to be performed after data acquisition to account
181 for this discrepancy. The excitation at this step starts at 1.1 s and ends at 16.1 s.
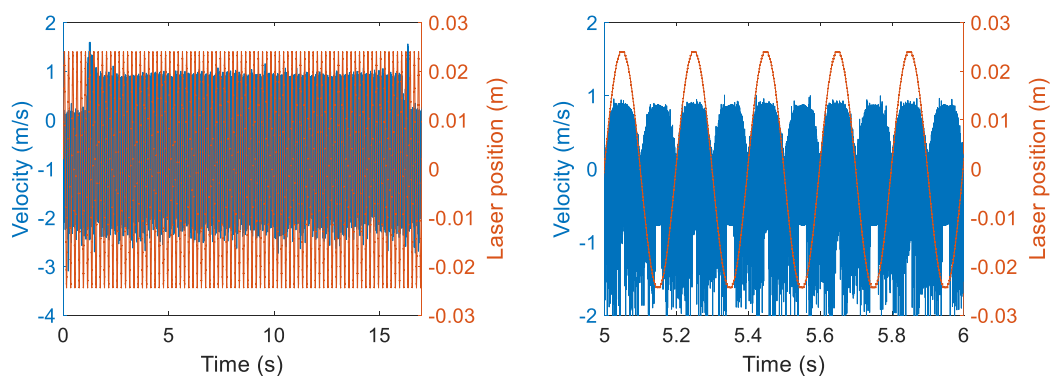

Figure 3: Measured velocity and laser beam position on a line on the sample over 17 seconds (left); Close-up view of time interval between 5 and 6 seconds (right).

182   Subsequently, at intervals of 0.4 seconds (equivalent to 2 complete mirror scans) with a 0.2-second overlap,
183 segments were subjected to separate analysis. This analysis includes the determination of the enveloped signal

through the application of a fast Fourier transform for approximately every five cycles of excitation, equivalent to 0.255 ms. This approach mitigates the impact of the speckle noise, ensuring a more accurate estimation of the envelope. Finally, the estimated envelope was smoothed using MATLAB's *smoothdata* function. This function employs a robust quadratic regression within a moving window, with a window size that attenuates approximately 25% of the energy of the input data. The final curve, depicted in Figure 4 for a duration of 0.4 s, provides the velocity of the sample at various time points, corresponding to distinct locations on the surface of the sample.
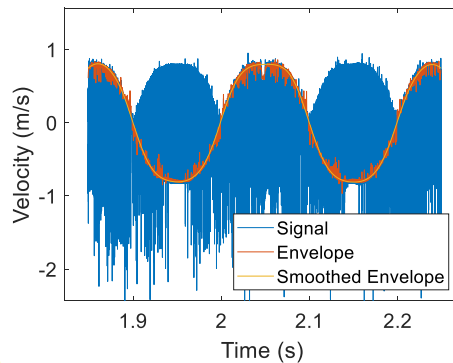

Figure 4: Smoothed envelope function of the measured velocity from the continuous scan signal. The envelope focuses on vibration of the sample while disregarding sidebands resulting from the continuous scan.

As mentioned in Section 2.2.1, the excitation frequency of the ultrasonic transducer is not precisely 20 kHz across the experiments. Figure 5 visually depicts the actual excitation frequency of the transducer, recorded by the NexTgen software, during the first step of the experiment.
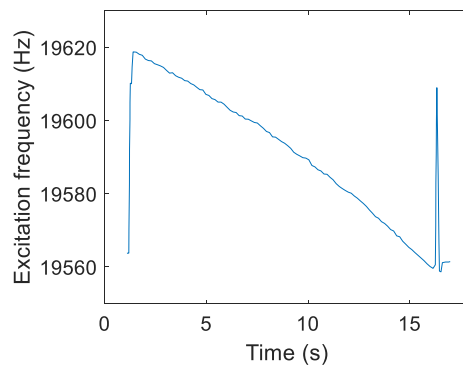

Figure 5: Excitation frequency of the high-power ultrasonic transducer derived from the NexTgen software. The excitation starts at 1.1 s with 15% power and goes on for 15 s.

The imposed load on the specimen is presumed to be longitudinal, as illustrated in Figure 6. The displacement at any location within the sample is regarded as constant across each cross-section and is a function of both time (t) and the position along the sample's length (x). This displacement at the start of the test, before the material heats up, can be presented by the following equation:

$$u(x,t) = u_0 \cos(\omega_s x - \varphi_s) \cos(\omega_f t - \varphi_f) \tag{3}$$

198 with
199   - u_0 the amplitude of the load
200   - ω_s the spatial angular frequency, calculated using $\omega_s = 2\pi/L_n$, and L_n the deformation wavelength,
201   which is approximately twice the length of the specimen at its first longitudinal mode.
202   - ω_f the angular frequency, $\omega_f = 2\pi f$, with f the loading frequency
203   - φ_s and φ_f the spatial and temporal phases, respectively
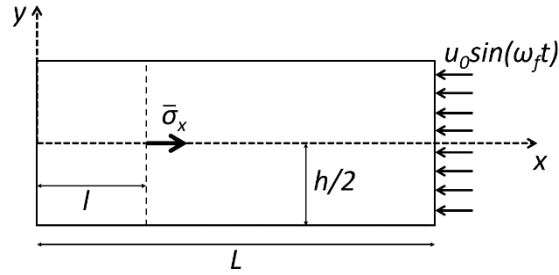

Figure 6: Schematical view of the sample under longitudinal sinusoidal loading.

204   As demonstrated above, the SLDV provides the velocity of the sample along a designated line over time.
205 Subsequently, this signal was employed to calculate displacement and acceleration signals using time derivation
206 and integration. To estimate the vibration over the sample at any given instant, the assumption was made that the
207 temperature at any point on the material remained constant during half of the mirror's cycle (equivalent to one full
208 line scan across the sample). This assumption holds valid given that the temperature variation within this time
209 interval (0.1 seconds) remained negligible. Indeed, the mean temperature elevation at the center of the sample
210 within this period amounted to 0.3°C across all steps, with a maximum of 0.5°C observed during Step 5. In order
211 to minimize this temperature variation, the option of increasing the frequency of the galvo scanner or decreasing
212 the power of the ultrasonic transducer was considered. Eventually, these experiments were conducted at 15%
213 power, which was the minimum value to generate clear harmonic signals using this system. It is worth noting that
214 further reducing the power could also affect the measurement duration and signal to noise ratio. Additionally,
215 increasing the frequency of the galvo scanner could introduce more speckle noise to the continuous laser scanning
216 measurements [21]. Therefore, a balance must be struck between this assumption and the influence of signal noise.
217   Afterwards, the partial derivative of the displacement along the sample at any time was computed using finite
218 difference differentiation to find the strain (ε_x) and strain rate ($\dot{\varepsilon}_x$). Finally, the average stress distribution along the
219 length of the sample was estimated as follows [6]:

$$\overline{\sigma_{xx}}(x,t) = -\rho x\, \overline{a_x}(x,t) \tag{4}$$

220 with $\overline{\sigma_{xx}}(x,t)$ the average Cauchy stress over the transverse section coordinate y, ρ the material density, and
221 $\overline{a_x}(x,t)$ the surface average of the longitudinal acceleration between the free edge and the considered section at
222 coordinate x. This equation is valid assuming that strain and material properties are uniform across the width at
223 each x position, and that the acceleration field only depends on x. Additionally, since the selected scan line on the
224 sample did not cover the whole sample until the edge, the acceleration profile on the scan line was extrapolated
225 using MATLAB *fit* function and a cubic polynomial model to calculate $\overline{a_x}(x,t)$ accurately.

226 Using stress and strain at different locations along the measuring line, the complex modulus of the material at
227 different temperatures and strain rates was estimated. These values were then shifted using the Arrhenius equation
228 and fitted to a conventional symmetric sigmoidal function, according to Equations 5 and 6.

$$\log|E^*| = \delta + \frac{\alpha}{1 + e^{\beta + \gamma \log S_r}} \tag{5}$$

$$\alpha_T = \exp\left(\frac{\Delta H}{R}\left(\frac{1}{T} - \frac{1}{T_r}\right)\right) \tag{6}$$

229 with E^* the complex modulus, δ the value of the lower asymptote, α the difference between values of the upper and
230 lower asymptotes, β and γ shape coefficients, S_r the reduced strain rate, α_T the shift factor as a function of
231 temperature, ΔH the activation energy associated with mechanism of internal friction, $R = 8.3144598$ J.mol^{-1}.K^{-1}
232 the gas constant, and T_r the reference temperature.
233 In order to have the temperature corresponding to each E^*, the acquired IR camera images were imported into
234 MATLAB. Figure 7 shows an IR image captured after 14 seconds into the initial experimental phase. This image
235 was first oriented horizontally and then the average temperature was computed for each vertical line, yielding an
236 average vertical temperature profile along the sample. In this step, it is assumed that the temperature is uniform
237 across any cross-section of the material, and that thermal conduction between the thin paint coating and the sample
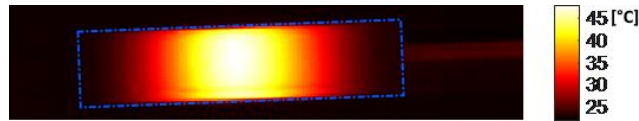238 equalizes their temperatures.
239

Figure 7: Example of an IR camera image captured near the end of the
excitation in step 1. As anticipated, the temperature of the sample exhibited
an elevation at its center, while remaining close to the room temperature on
the sides.

240

3. Results and discussion

3.1. IR camera results

Figure 8 presents the temperature profile along the sample at 1-second intervals during the first step of the experiment. As anticipated, self-heating induces a temperature increase at the center of the sample, while the temperature on the edges remained near room temperature. This provides the opportunity to relate the calculated properties at different locations to different temperatures.
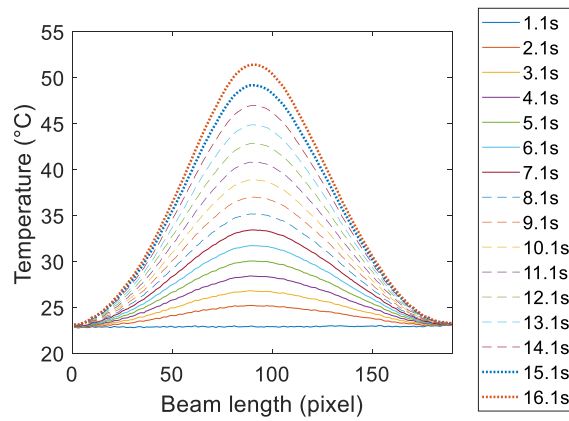

Figure 8: Temperature profile along the beam at 1-second intervals, starting from 1.1 s when the excitation force of step 1 started. It shows how the temperature at the middle of the beam increased while the temperature on the sides remained almost constant.

Figure 9 presents a similar temperature profile across the beam at both the initiation and end of each step. It is important to highlight that the analysis of this study was limited to temperatures up to 95°C. Beyond this temperature, nonlinearities emerged, requiring an alternate analysis approach. This can potentially be attributed to the proximity to the glass transition, which is beyond the scope of this article.
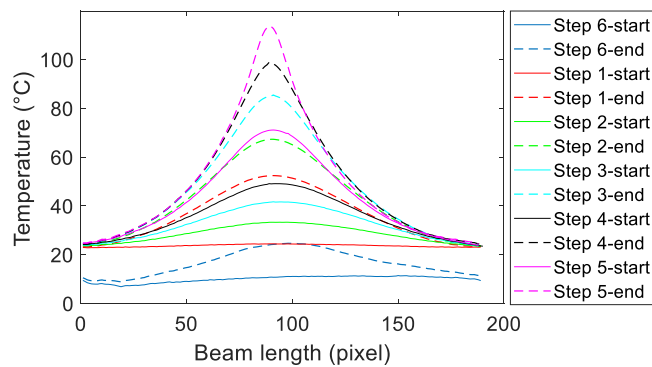

Figure 9: Temperature profile along the beam at the initial (solid lines) and end (dashed lines) of each step. Step 6 is the only step that includes a cooling stage.

254 *3.2. Velocity, displacement, strain, and strain-rate*

255 As explained in Section 2.4, the derived velocity and displacement profile of the sample can be plotted across
256 the length of the specimen at any point during the excitation. Figure 10 shows these profiles over the sample during
257 the first step of the experiments at 2.1±0.05 s. Given that the specimen was excited close to its first longitudinal
258 natural frequency, as anticipated from FEM simulations [19], the vibration reached its maximum at the edges of
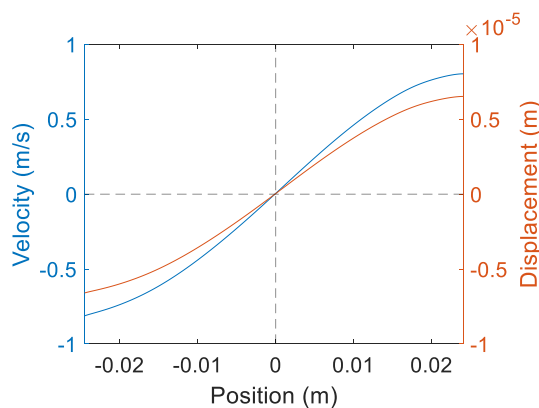259 the sample and remained minimal in the middle.
260

Figure 10: Measured velocity and displacement across the sample at 2.1±0.05 s. Position 0 corresponds to the midpoint of the sample, with the ultrasonic transducer connected to the positive side.

261 Using this displacement profile, strain and strain rate across the sample were computed. An example of strain
262 and strain rate profile, derived from the displacement illustrated in Figure 10, is presented in Figure 11a. As
263 predicted from beam simulations, at the start of the experiments, both values exhibit their peak magnitude near the
264 center of the sample and are at their minimum at the sides. Approximately 90 data points from each step of the
265 experiments, within the region delimited by the vertical dashed lines, were selected for subsequent calculation of
266 the complex modulus magnitude. The strain profiles illustrated in Figure 11b represent the end of each step, with
267 an exception for step 5, where the last measurements before the temperature surpassed 95°C were selected. The
268 strain exhibits similarity across different steps, gradually decreasing over time on the side connected to the
269 transducer. As the temperature at the center approaches the T_g, the changes in the strain become more pronounced.
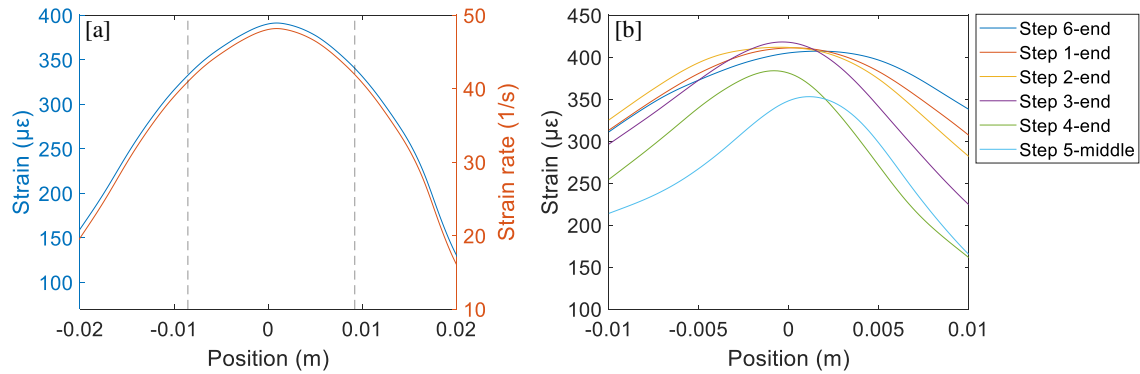
Figure 11: [a] Strain and strain rate calculations across the sample at 2.1±0.05 seconds. [b] Strain profile at different steps; Position 0 corresponds to the midpoint of the sample, with the ultrasonic transducer linked to the positive side. Vertical dashed lines delimit the region used for determining the magnitude of the complex modulus.

3.3. Acceleration and stress

The acceleration along the scan line was derived from the velocity profile. To obtain the $\overline{a_x}(x,t)$ needed for Eq. 6, a curve was fitted to the acceleration profile, as presented in Figure 12a. Subsequently, Eq. 4 was utilized to determine the stress profile on the sample (see Figure 12a). Consistent with the observations using cameras and grid method in the literature [6], Figure 12 shows a decline in the stress profile as the experiment progresses and the temperature in the center of the material increases.
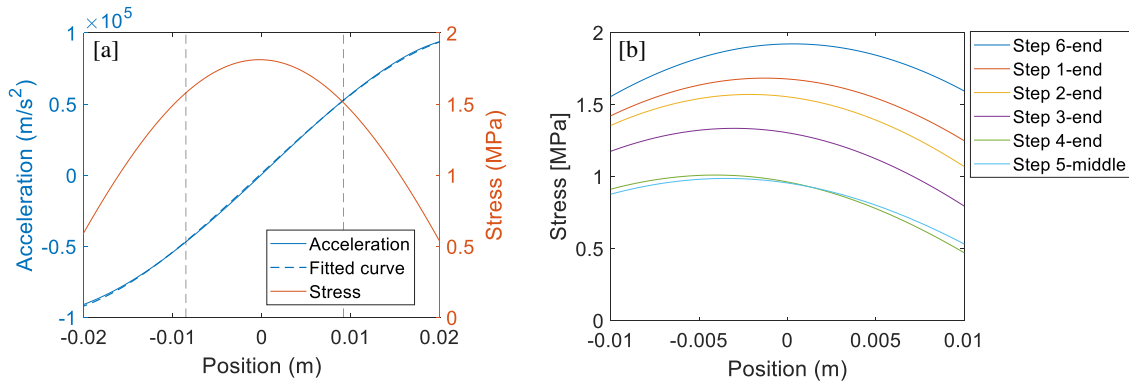

Figure 12: [a] Acceleration profile, fitted acceleration curve and calculated stress across the sample at 2.1±0.05 seconds. The vertical dashed lines delimit the region used for determining the amplitude of the complex modulus. [b] Stress profile at different steps.

3.4. Complex modulus master curve

The magnitude of the complex modulus was determined for 458 data points across various temperatures and strain rates during the five experiment steps, as depicted in Figure 13. The temperature spanned from 10 to 95°C, while the strain rate ranged from 28.55 to 54.29 1/s. It should be noted that this strain rate represents the peak strain rate at a specific point on the sample at a particular cycle and is not equivalent to the strain rate in quasi-static tests. |E*| exhibited variations within the range of 2.49 to 5.28 GPa in these temperature and strain rate ranges. This

283 figure clearly demonstrated the temperature dependency of |E*|. Any vertical line on this figure signifies an increase
284 of |E*| from below 3.4 GPa to above 4.9 GPa when transitioning from highest to lowest temperatures. Additionally,
285 |E*| displayed a general growth at higher strain rates. However, this growth was relatively smaller. This outcome
286 is consistent with expectations, given the relatively narrow range of the strain rates during these experiments. To
287 expand the range of tested strain rates, it is possible to increase the power of the ultrasonic transducer, as
288 demonstrated in experiments conducted by [6], where strain rates of up to 200 1/s were attained. However, this
289 change requires a higher frequency for the galvo scanner to enable faster measurements and manage the resulting
290 increase in temperature change rate (refer to the assumption discussed regarding the temperature change of the
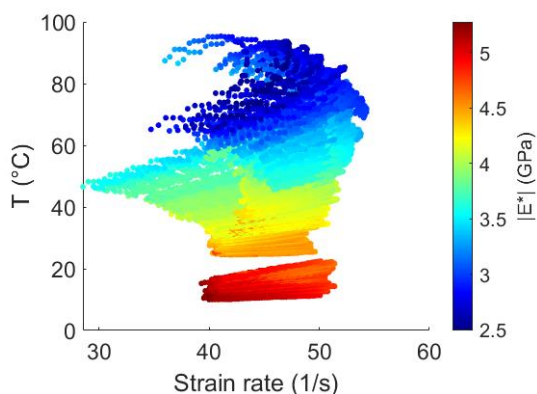291 sample in Section 2.4).
292

Figure 13: Magnitude of complex modulus of the tested PMMA sample, at 458 distinct combinations of temperatures and strain rates.

293   Figure 14 shows the master curve of the material at 25°C and the shifted data points used to construct the curve.
294 The dashed curves represent a ±10% vertical variation around the master curve, aiding in the visual assessment of
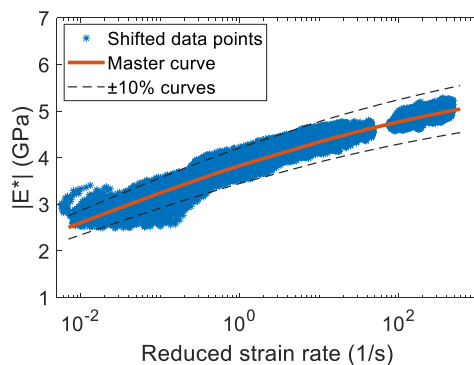295 result variability.

Figure 14: Master curve of the PMMA sample at 25°C and the shifted data points employed to construct the master curve. The dashed lines illustrate the ±10% variation from the master curve, aiding in visual comparison and assessment.

296

297   Figure 15 displays the same master curve at 25°C, accompanied by three additional curves obtained from distinct
298   experiments documented in the literature. The master curve generated from the proposed tests in this study closely
299   aligns with the curve produced by [22]. In their work, Richeton *et al.* employed both quasi-static uniaxial
300   compression tests and dynamic uniaxial compression tests, utilizing a split Hopkinson pressure bar setup, to
301   construct the master curve of PMMA across a wide spectrum of strain rates spanning from 10^{-4} to 5000 1/s [23].

302   Overall, the trends observed in all the curves exhibit similarities, with two notable differences. The first
303   difference exists between the Dynamic Mechanical Thermal Analysis (DMTA) tests conducted by [6] and the
304   remaining curves, particularly at high reduced strain rates. |E*| at high reduced strain rates, which is shifted data
305   from low temperatures (as low as -80°C), shows lower values than the results obtained from actual high strain rate
306   tests obtained from other testing methods. The second notable distinction emerges in the comparison between the
307   master curve derived from ultrasonic experiments proposed by [6] and the other curves. This curve exhibits lower
308   values in the high-temperature, low-strain-rate region and elevated values in the low-temperature, high-strain-rate
309   region. This aligns with the anticipated differences between this curve and the DMTA results since the temperature
310   and the strain rate ranges used in the experiments were different. However, it is not fully supported by the curves
311   obtained through the proposed technique in this study, nor with the methodology employed by Richeton *et al.* [22].
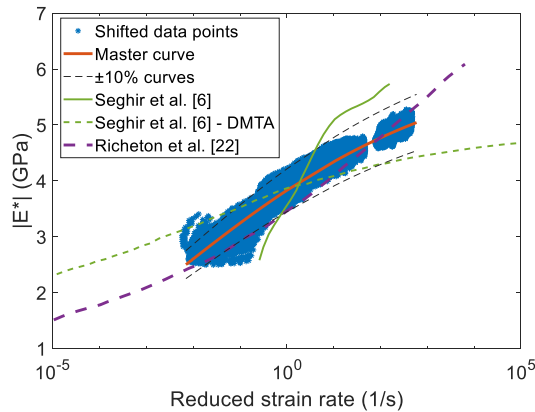

Figure 15: Shifted data points (to 25°C) and the master curve constructed in this study (extrapolated on both sides) compared with the data from ultrasonic and DMTA tests performed by Seghir *et al.* [6], and the experiments conducted by Richeton *et al.* [22].

312

313   **4. Conclusions**

      In this study, a pioneering technique for estimating the master curve of the complex modulus of a viscoelastic
material was successfully introduced. The novel approach overcomes the limitations of conventional methods by
taking advantage of the capabilities of various optical measurement systems to characterize material properties
across different locations quickly. The strategy involved utilizing a high-power ultrasonic transducer, operating at
approximately 20 kHz, close to the specimen's first longitudinal natural frequency therefore exciting it on its first
longitudinal mode. This excitation induced varying temperature distributions, caused by self-heating, and strain
rates across the sample.

      Meanwhile, a scanning laser Doppler vibrometer was deployed to continuously acquire the vibrational response
of the sample on a predefined line. A novel analysis technique was developed in MATLAB to analyze the data and
determine the magnitude of the complex modulus of the material under different conditions. This data was then

correlated with temperature measurements obtained via an infrared camera. This approach facilitated the establishment of a broad temperature range spanning from 6 to 117°C, coupled with strain rates of up to 54.3 1/s along the sample. The constructed master curve closely aligned with that of the quasi-static uniaxial compression tests and dynamic uniaxial compression tests found in the literature. Additionally, similar to previous research, the proposed method highlighted the increase in complex modulus at elevated reduced strain rates, which is less obvious in DMTA results.

By merging optical measurement technologies with an innovative experimental approach, this study significantly contributes to the understanding of viscoelastic material behavior, offering promising avenues for further exploration and application. Future investigations could involve extending the technique to a wider range of samples and materials, thereby assessing the repeatability and reproducibility of this method. Increasing the power of the ultrasonic transducer could help measure even at higher strain rates and requires capturing data with a faster galvo scanner. Finally, exploring analysis techniques that use a denser distribution of data points along the sample, particularly near the edges where lower strains can result in noisier measurements, would be a valuable avenue to pursue.

Acknowledgements

Declaration of generative AI and AI-assisted technologies in the writing process

During the preparation of this work, the authors used GPT-3.5 in order to enhance the quality of writing and grammar. After using this tool, the authors reviewed and edited the content as needed and take full responsibility for the content of the publication.

References

[1] A.D. Mulliken, M.C. Boyce, Mechanics of the rate-dependent elastic-plastic deformation of glassy polymers from low to high strain rates, Int J Solids Struct 43 (2006) 1331–1356. https://doi.org/10.1016/j.ijsolstr.2005.04.016.

[2] W. Grellmann, S. Seidler, Polymer Testing, Carl Hanser Verlag, Munich, Germany, 2022. https://doi.org/10.3139/9781569908075.

[3] C.R. Siviour, J.L. Jordan, High Strain Rate Mechanics of Polymers: A Review, Journal of Dynamic Behavior of Materials 2 (2016) 15–32. https://doi.org/10.1007/s40870-016-0052-8.

[4] F. Pierron, Material Testing 2.0: A brief review, Strain (2023) 1–20. https://doi.org/10.1111/str.12434.

[5] F. Pierron, M. Grédiac, Towards Material Testing 2.0. A review of test design for identification of constitutive parameters from full-field measurements, Strain 57 (2021) 1–22. https://doi.org/10.1111/str.12370.

[6] R. Seghir, F. Pierron, A Novel Image-based Ultrasonic Test to Map Material Mechanical Properties at High Strain-rates, Exp Mech 58 (2018) 183–206. https://doi.org/10.1007/s11340-017-0329-4.

[7] R. Moulart, F. Pierron, S.R. Hallett, M.R. Wisnom, Full-Field Strain Measurement and Identification of Composites Moduli at High Strain Rate with the Virtual Fields Method, Exp Mech 51 (2011) 509–536. https://doi.org/10.1007/s11340-010-9433-4.

[8] M. Kucher, M. Dannemann, D. Peyrow Hedayati, R. Böhm, N. Modler, Experimental Investigation of the Vibration-Induced Heating of Polyetheretherketone for High-Frequency Applications, Solids 4 (2023) 116–132. https://doi.org/10.3390/solids4020008.

343 [9] G.M.D. Almaraz, A.G. Martínez, R.H. Sánchez, E.C. Gómez, M.G. Tapia, J.C.V. Juárez, Ultrasonic
344   Fatigue Testing on the Polymeric Material PMMA, Used in Odontology Applications, Procedia Structural
345   Integrity 3 (2017) 562–570. https://doi.org/10.1016/j.prostr.2017.04.039.
346 [10] M. Mihalec, J. Javh, F. Cianetti, M. Moretti, G. Rossi, J. Slavič, M. Boltežar, Damping heat coefficient –
347   Theoretical and experimental research on a vibrating beam, J Sound Vib 400 (2017) 13–21.
348   https://doi.org/10.1016/j.jsv.2017.04.023.
349 [11] N. Hasheminejad, C. Vuye, A. Margaritis, W. Van den bergh, J. Dirckx, S. Vanlanduit, Characterizing the
350   complex modulus of asphalt concrete using a scanning laser doppler vibrometer, Materials 12 (2019) 1–
351   18. https://doi.org/10.3390/ma12213542.
352 [12] N. Hasheminejad, C. Vuye, A. Margaritis, W. Van den bergh, J. Dirckx, S. Vanlanduit, Identification of
353   the viscoelastic properties of an asphalt mixture using a scanning laser Doppler vibrometer, Mater Struct
354   53 (2020). https://doi.org/10.1617/s11527-020-01567-9.
355 [13] D.A. Ehrhardt, M.S. Allen, S. Yang, T.J. Beberniss, Full-field linear and nonlinear measurements using
356   Continuous-Scan Laser Doppler Vibrometry and high speed Three-Dimensional Digital Image Correlation,
357   Mech Syst Signal Process 86 (2017) 82–97. https://doi.org/10.1016/j.ymssp.2015.12.003.
358 [14] N. Hasheminejad, C. Vuye, W. Van den bergh, J. Dirckx, J. Leysen, S. Sels, S. Vanlanduit, Identification
359   of pavement material properties using a scanning laser Doppler vibrometer, in: AIP Conf Proc, 2016: p.
360   070005. https://doi.org/10.1063/1.4952682.
361 [15] S. Yang, D. Ehrhardt, M.S. Allen, A Review of Signal Processing Techniques for Continuous-Scan Laser
362   Doppler Vibrometry, in: Proceedings of the ASME 2014 International Design Engineering Technical
363   Conferences & Computers and Information in Engineering Conference, Buffalo, New York, USA, 2014.
364 [16] A.B. Stanbridge, D.J. Ewins, Modal Testing Using a Scanning Laser Doppler Vibrometer, Mech Syst
365   Signal Process 13 (1999) 255–270. https://doi.org/10.1006/mssp.1998.1209.
366 [17] D. Di Maio, P. Castellini, M. Martarelli, S. Rothberg, M.S. Allen, W.D. Zhu, D.J. Ewins, Continuous
367   Scanning Laser Vibrometry: A raison d'être and applications to vibration measurements, Mech Syst Signal
368   Process 156 (2021) 107573. https://doi.org/10.1016/j.ymssp.2020.107573.
369 [18] N. Hasheminejad, C. Vuye, W. Van den bergh, J. Dirckx, S. Vanlanduit, A Comparative Study of Laser
370   Doppler Vibrometers for Vibration Measurements on Pavement Materials, Infrastructures (Basel) 3 (2018)
371   47. https://doi.org/10.3390/infrastructures3040047.
372 [19] N. Hasheminejad, C. Vuye, S. Vanlanduit, Identification of the viscoelastic properties of bituminous mortar
373   using vibration measurements, in: In Proceedings of the International Seminar on Model Analysis/KUL.
374   Faculty of Applied Sciences. Department of Mechanical Engineering, Production Engineering, Machine
375   Design and Automation., Leuven, 2022: pp. 1010–1019.
376 [20] M. Martarelli, Exploiting the laser scanning facility for vibration measurements, Imperial College of
377   Science, Technology & Medicine, University of London, 2001.
378 [21] M. Martarelli, D.J. Ewins, Continuous scanning laser Doppler vibrometry and speckle noise occurrence,
379   Mech Syst Signal Process 20 (2006) 2277–2289. https://doi.org/10.1016/j.ymssp.2005.06.003.
380 [22] J. Richeton, G. Schlatter, K.S. Vecchio, Y. Rémond, S. Ahzi, A unified model for stiffness modulus of
381   amorphous polymers across transition temperatures and strain rates, Polymer (Guildf) 46 (2005) 8194–
382   8201. https://doi.org/10.1016/j.polymer.2005.06.103.
383 [23] J. Richeton, S. Ahzi, K.S. Vecchio, F.C. Jiang, R.R. Adharapurapu, Influence of temperature and strain
384   rate on the mechanical behavior of three amorphous polymers: Characterization and modeling of the
385   compressive   yield   stress,   Int   J   Solids   Struct   43   (2006)   2318–2335.
386   https://doi.org/10.1016/j.ijsolstr.2005.06.040.
387